

Higher-Order Nonlinear Anomalous Hall Effects Induced by Berry Curvature Multipoles

Cheng-Ping Zhang^{1,*}, Xue-Jian Gao^{1,*}, Ying-Ming Xie¹, Hoi Chun Po², and K. T. Law^{1†}

¹*Department of Physics, Hong Kong University of Science and Technology, Clear Water Bay, Hong Kong, China and*

²*Department of Physics, Massachusetts Institute of Technology, Cambridge, Massachusetts, USA*

In recent years, it had been shown that Berry curvature monopoles and dipoles play essential roles in the anomalous Hall effect and the nonlinear Hall effect respectively. In this work, we demonstrate that Berry curvature multipoles (the higher moments of Berry curvatures at the Fermi energy) can induce higher-order nonlinear anomalous Hall (NLAH) effect. Specifically, an *ac* Hall voltage perpendicular to the current direction emerges, where the frequency is an integer multiple of the frequency of the applied current. Importantly, by analyzing the symmetry properties of all the 3D and 2D magnetic point groups, we note that the quadrupole, hexapole and even higher-order Berry curvature moments can cause the leading-order frequency multiplication in certain materials. To provide concrete examples, we point out that the third-order NLAH voltage can be the leading-order Hall response in certain antiferromagnets due to Berry curvature quadrupoles, while the fourth-order NLAH can be the leading response in the surface states of topological insulators induced by Berry curvature hexapole. Our results are established by symmetry analysis, effective Hamiltonian and first-principles calculations. Other materials that support the NLAH effect are further proposed, including 2D antiferromagnets and ferromagnets, Weyl semimetals and twisted bilayer graphene near the quantum anomalous Hall phase.

Introduction.—The Hall effect is a fascinating phenomenon that a Hall voltage perpendicular to the applied current direction can be generated under an external magnetic field. In ferromagnets, a Hall voltage can be created in the absence of an external magnetic field, which is known as the anomalous Hall effect. It has an intrinsic contribution from the Berry curvature monopole which is the integration of Berry curvature over occupied states [1, 2]. Recently, anomalous Hall effects are also discovered in antiferromagnets [3–8].

Surprisingly, it was pointed out recently that a Hall voltage can be induced even in time-reversal invariant systems [9], in which the generated Hall voltage doubles the frequency of the applied *ac* electric current. This so-called nonlinear Hall effect is induced by the Berry curvature dipole, which is the first-order moment of the Berry curvature over occupied states. The nonlinear Hall effect has been observed experimentally in bilayer and multi-layer WTe₂ [10, 11] and more recently in twisted WSe₂ [12, 13]. However, in principle, higher-order Berry curvature moments can be non-vanishing and their physical consequences are not known.

In this work, we provide a general theory for higher-order nonlinear anomalous Hall (NLAH) effects which can be induced by the Berry curvature multipoles such as quadrupole [14], hexapole and higher-order moments. Specifically, an *ac* Hall voltage with frequency which is an integer multiple of the frequency of the applied *ac* current can be generated by Berry curvature multipoles. The higher-order effects are generally expected to be small compared to lower-order effects. However, we point out that Berry curvature quadrupole, hexapole and even higher-order moments can cause the leading-order effects when lower-order Berry curvature moments are forced

to vanish by crystal symmetry. Magnetic point groups (MPGs) which allow higher-order Berry curvature moments to be the leading-order moments are listed in Table I and Table II respectively for three-dimensional (3D) and two-dimensional (2D) materials. To give concrete examples, we point out that in antiferromagnets such as monolayer SrMnBi₂, the NLAH effect induced by Berry curvature quadrupole is the leading-order Hall response, as both the anomalous Hall and the nonlinear Hall effect are prohibited by symmetry. Furthermore, with a current easily accessible in experiments, the third-order NLAH voltage can be of the order $\sim 10 \mu\text{V}$, which is comparable with the nonlinear Hall voltage in WTe₂ [10, 11]. We further point out that the surface states of topological insulators with C_{3v} symmetry support fourth-order NLAH effect due to the non-vanishing hexapole which is the lowest order non-vanishing Berry curvature moment.

The rest of the paper is organized as follows. We first use the Boltzmann equation approach to establish the relationship between the *ac* conductivity and the Berry curvature multipoles. Second, the symmetry properties of the Berry curvature multipoles in all MPGs are analyzed and summarized in Table I and Table II. Third, to be specific, we show explicitly how the third-order NLAH effect induced by Berry curvature quadrupole becomes the leading-order Hall response in $4'mm'$ MPG (in Hermann-Mauguin notation [15]), which is the symmetry for monolayer antiferromagnet SrMnBi₂. We further show that the fourth-order NLAH effect induced by Berry curvature hexapole is the lowest order response in C_{3v} point group, and the theory applies to the surface states of topological insulators. The third-order NLAH effect may also be observed in other candidate materials, including 2D antiferromagnets and ferromagnets, Weyl

semimetals and twisted bilayer graphene near the quantum anomalous Hall phase.

Nonlinear conductivity and Berry curvature multipoles— In this section, we establish the connection between the nonlinear conductivity and Berry curvature multipoles using the Boltzmann equation approach [9, 14]. We focus only on the intraband contribution, which is valid when the frequency is much lower than the band gaps between adjacent bands. Recall the semiclassical equations of electron motion:

$$\frac{d}{dt}\mathbf{r} = \frac{1}{\hbar}\nabla_{\mathbf{k}}\varepsilon_{\mathbf{k}} + \frac{e}{\hbar}\mathbf{E} \times \boldsymbol{\Omega}, \quad (1)$$

$$\frac{d}{dt}\mathbf{k} = -\frac{e\mathbf{E}}{\hbar}, \quad (2)$$

where $\mathbf{E} = \mathbf{E}(t)$ is the time-dependent applied electric field and $\boldsymbol{\Omega}$ is the Berry curvature.

The electric current is given by the integral of physical velocity:

$$\mathbf{j}(t) = -e \int_{\mathbf{k}} f(\mathbf{k}, t) \frac{d\mathbf{r}}{dt}, \quad (3)$$

where $\int_{\mathbf{k}} = \int d^d k / (2\pi)^d$, and d is the dimensionality. The time evolution of distribution function $f(\mathbf{k}, t)$ is given by the Boltzmann equation:

$$\frac{d\mathbf{k}}{dt} \cdot \nabla_{\mathbf{k}} f(\mathbf{k}, t) + \partial_t f(\mathbf{k}, t) = \frac{f_0 - f(\mathbf{k}, t)}{\tau}, \quad (4)$$

where f_0 is the equilibrium Fermi-Dirac distribution function and τ represents the relaxation time.

With a harmonic electric field $\mathbf{E}(t) = \text{Re}\{E_{\alpha}e^{i\omega t}\hat{\mathbf{e}}_{\alpha}\}$ (Greek letters $\alpha, \beta, \gamma = x, y, z$ represent the spatial indices), the current response can be obtained order by order (see Supplemental Material [16] for details).

The first-order response is at the same frequency as the driving force: $j_{\mu}^{(1)}(t) = \text{Re}\{\sigma_{\mu\alpha}^{(1)}(\omega)E_{\alpha}e^{i\omega t}\}$, with

$$\sigma_{\mu\alpha}^{(1)}(\omega) = \frac{e^2}{\hbar} \int_{\mathbf{k}} f_0 \left(\frac{\partial_{\mu}\partial_{\alpha}\varepsilon_{\mathbf{k}}}{\hbar\tilde{\omega}} - \epsilon_{\mu\alpha\beta}\Omega_{\beta} \right), \quad (5)$$

where $\partial_{\alpha} = \partial/\partial k_{\alpha}$ and $\epsilon_{\mu\alpha\beta}$ is the Levi-Civita tensor. $\tilde{\omega}$ represents $i\omega + \gamma$ [17] and $\gamma = 1/\tau$. The first term is the usual Drude conductivity, which is symmetric with respect to the two indices: $\sigma_{\mu\alpha}^{(1),D}(\omega) = \sigma_{\alpha\mu}^{(1),D}(\omega)$. The second term is the intrinsic contribution to the anomalous Hall conductivity from the integration of Berry curvature $\int_{\mathbf{k}} f_0 \Omega_{\beta}$, which can be viewed as Berry curvature monopole. The anomalous Hall conductivity is defined as the antisymmetric part of the conductivity tensor: $\sigma_{\mu\alpha}^{(1),H}(\omega) = -\sigma_{\alpha\mu}^{(1),H}(\omega)$, which vanishes when time-reversal symmetry is present, as required by Onsager reciprocal relation [1]. As an analogy, we define the NLAH conductivity as the antisymmetric part of the nonlinear conductivity tensor following ref. [18], in order to distinguish it from the Drude-like contribution.

The second-order response consists of a rectified current and a second harmonic generation: $j_{\mu}^{(2)}(t) = \text{Re}\{\sigma_{\mu\alpha\beta}^{(2)}(0)E_{\alpha}E_{\beta}^{*} + \sigma_{\mu\alpha\beta}^{(2)}(2\omega)E_{\alpha}E_{\beta}e^{2i\omega t}\}$, with

$$\sigma_{\mu\alpha\beta}^{(2)}(0) = -\frac{e^3}{2\hbar^3} \int_{\mathbf{k}} f_0 \frac{\partial_{\mu}\partial_{\alpha}\partial_{\beta}\varepsilon_{\mathbf{k}}}{\gamma\tilde{\omega}} + \frac{e^3}{2\hbar^2} \frac{\epsilon_{\mu\alpha\gamma}}{\tilde{\omega}} D_{\beta\gamma}, \quad (6)$$

$$\sigma_{\mu\alpha\beta}^{(2)}(2\omega) = -\frac{e^3}{2\hbar^3} \int_{\mathbf{k}} f_0 \frac{\partial_{\mu}\partial_{\alpha}\partial_{\beta}\varepsilon_{\mathbf{k}}}{\tilde{\omega}(2\omega)} + \frac{e^3}{2\hbar^2} \frac{\epsilon_{\mu\alpha\gamma}}{\tilde{\omega}} D_{\beta\gamma}. \quad (7)$$

Each conductivity tensor contains two terms. The first term is the Drude-like contribution and the second term is the NLAH conductivity induced by Berry curvature dipole $D_{\alpha\beta} = \int_{\mathbf{k}} f_0 \partial_{\alpha}\Omega_{\beta}$. The second term is the origin of the nonlinear Hall effect first pointed out by Sodemann and Fu [9] which has attracted many theoretical and experimental studies in recent years [10–13, 19–25].

In this work, we focus on the higher-order responses which importantly can be the leading-order responses under certain MPG symmetries as detailed in the following sections. The third-order response is composed of currents at both fundamental and third harmonic frequencies: $j_{\mu}^{(3)}(t) = \text{Re}\{\sigma_{\mu\alpha\beta\gamma}^{(3)}(\omega)E_{\alpha}E_{\beta}E_{\gamma}^{*}e^{i\omega t} + \sigma_{\mu\alpha\beta\gamma}^{(3)}(3\omega)E_{\alpha}E_{\beta}E_{\gamma}e^{3i\omega t}\}$, with

$$\sigma_{\mu\alpha\beta\gamma}^{(3)}(\omega) = \frac{3e^4}{4\hbar^4} \int_{\mathbf{k}} f_0 \frac{\partial_{\mu}\partial_{\alpha}\partial_{\beta}\partial_{\gamma}\varepsilon_{\mathbf{k}}}{\tilde{\omega}(-\tilde{\omega})(2\omega)} - \frac{e^4}{4\hbar^3} \left[\frac{2\epsilon_{\mu\alpha\delta}}{\tilde{\omega}(-\tilde{\omega})} Q_{\beta\gamma\delta} + \frac{\epsilon_{\mu\gamma\delta}}{\tilde{\omega}(2\omega)} Q_{\alpha\beta\delta} \right], \quad (8)$$

$$\sigma_{\mu\alpha\beta\gamma}^{(3)}(3\omega) = \frac{e^4}{4\hbar^4} \int_{\mathbf{k}} f_0 \frac{\partial_{\mu}\partial_{\alpha}\partial_{\beta}\partial_{\gamma}\varepsilon_{\mathbf{k}}}{\tilde{\omega}(2\omega)(3\omega)} - \frac{e^4}{4\hbar^3} \frac{\epsilon_{\mu\alpha\delta}}{\tilde{\omega}(2\omega)} Q_{\beta\gamma\delta}. \quad (9)$$

The first term is the Drude-like contribution and the second term is the NLAH conductivity induced by Berry curvature quadrupole [14], which is defined as

$$Q_{\alpha\beta\gamma} = \int_{\mathbf{k}} f_0 \partial_{\alpha}\partial_{\beta}\Omega_{\gamma}. \quad (10)$$

It can be generalized to multi-band cases by summing up the contributions from all bands. The quadrupole can also be rewritten as

$$Q_{\alpha\beta\gamma} = - \int_{\mathbf{k}} (\partial_{\alpha}\varepsilon_{\mathbf{k}})(\partial_{\beta}\Omega_{\gamma})f_0'(\varepsilon_{\mathbf{k}} - \mu), \quad (11)$$

which indicates that the NLAH effect induced by Berry curvature quadrupole is a Fermi liquid property. Similarly, the Berry curvature hexapole is defined as

$$H_{\alpha\beta\gamma\delta} = \int_{\mathbf{k}} f_0 \partial_{\alpha}\partial_{\beta}\partial_{\gamma}\Omega_{\delta}, \quad (12)$$

TABLE I. Leading-order intrinsic anomalous Hall response in all the 122 3D magnetic point groups

leading-order response	magnetic point groups
No anomalous Hall response	$\bar{1}1', \bar{1}', 2/m1', 2'/m, 2/m', mmm1', m'mm, m'm'm', 4/m1' 4/m', 4'/m', 4/mmm1', 4/m'mm, 4'/m'm'm, 4/m'm'm', \bar{3}1', \bar{3}', \bar{3}m1', \bar{3}'m, \bar{3}'m', 6/m1', 6'/m, 6/m', 6/mmm1', 6/m'mm, 6'/mmm', 6/m'm'm', m\bar{3}1', m'\bar{3}', m\bar{3}m1', m'\bar{3}'m, m'\bar{3}'m'$
1st-order	$1, \bar{1}, 2, 2', m, m', 2/m, 2'/m', 2'2'2, m'm2', m'm'2, m'm'm, 4, \bar{4}, 4/m, 42'2', 4m'm', \bar{4}2'm', 4/mm'm', 3, \bar{3}, 32', 3m', \bar{3}m', 6, \bar{6}, 6/m, 62'2', 6m'm', \bar{6}m'2', 6/mm'm'$
2nd-order	$11', 21', m1', 222, 2221', mm2, mm21', 41', 4', \bar{4}1', \bar{4}', 422, 4221', 4'22', 4mm, 4mm1', 4'm'm, \bar{4}2m, \bar{4}2m1', \bar{4}2'm, \bar{4}2m', 622, 6221', 6'22', 6mm, 31', 32, 321', 3m, 3m1', 61', 6', 6mm1', 6'mm', 23, 231', 432, 4321', 4'32'$
3rd-order	$mmm, 4'/m, 4/mmm, 4'/mmm', \bar{3}m, \bar{6}', 6'/m', \bar{6}m2, \bar{6}'m'2, \bar{6}'m2', 6/mmm, 6'/m'mm', m\bar{3}, \bar{4}'3m', m\bar{3}m'$
4th-order	$\bar{6}1', \bar{6}m21', \bar{4}3m, \bar{4}3m1'$
5th-order	$m\bar{3}m$

and the higher-order moments can be defined in a similar manner. The higher-order nonlinear conductivities and their relations to higher-order Berry curvature moments can be found in the Supplemental Material [16].

Symmetry analysis of Berry curvature multipoles—As shown in the last section, Berry curvatures contribute to the higher-order conductivity in general [14]. In this section, we analyze the symmetry properties of Berry curvature multipoles. Taking the Berry curvature quadrupole as an example, we point out that time-reversal symmetry forces the Berry curvature quadrupoles to be zero. However, for materials belonging to 66 (out of the 122) MPGs which break time-reversal symmetry, the Berry curvature quadrupole can be finite. Moreover, in 15 MPGs as listed in Table I, the quadrupole is the lowest order non-vanishing Berry curvature moment.

To have finite Berry curvature quadrupole, we note that under time-reversal symmetry \mathcal{T} : $\partial_\alpha \rightarrow -\partial_\alpha$ and $\Omega_\gamma \rightarrow -\Omega_\gamma$ and therefore, according to Eq. 10, the Berry curvature quadrupole vanishes. As a result, only materials which break time-reversal symmetry can have transport responses induced by Berry curvature quadrupoles. Under general spatial symmetries, since the Berry curvature is a pseudovector, the Berry curvature quadrupole transforms as a rank-3 pseudotensor. Therefore a symmetry operation Λ imposes constraint on the form of the quadrupole:

$$Q_{\alpha\beta\gamma} = \pm \det(\Lambda) \Lambda_{\alpha\alpha'} \Lambda_{\beta\beta'} \Lambda_{\gamma\gamma'} Q_{\alpha'\beta'\gamma'}, \quad (13)$$

where $+$ ($-$) is taken for unitary(antiunitary) operations. Furthermore, the quadrupole is symmetric with respect

to the first two indices: $Q_{\alpha\beta\gamma} = Q_{\beta\alpha\gamma}$ as indicated by Eq. 10, because the order of derivatives are interchangeable.

From above, we note that the Berry curvature quadrupole transforms exactly the same as piezomagnetic tensor $\chi_{\alpha\beta\gamma}$, which generates a magnetization $M_\gamma = \chi_{\alpha\beta\gamma} \mathcal{E}_{\alpha\beta}$ when a strain $\mathcal{E}_{\alpha\beta}$ is applied. Because the magnetization is a pseudovector and strain is a symmetric tensor, the piezomagnetic tensor is also a rank-3 pseudotensor with the first two indices to be symmetric $\chi_{\alpha\beta\gamma} = \chi_{\beta\alpha\gamma}$. Out of the 122 MPGs, 66 of them are piezomagnetic [26] and therefore support nonzero Berry curvature quadrupoles, whose explicit forms are listed in the Supplemental Material [16].

Among the 66 MPGs with Berry curvature quadrupoles, 31 of them have finite Berry curvature monopoles and 20 of them have Berry curvature dipoles as the lowest order non-vanishing moment. Importantly, as listed in Table I, there are 15 MPGs in which the Berry curvature quadrupole is the leading non-vanishing moment.

The same analysis can be applied to the higher-order Berry curvature moments. In general for all the 122 3D MPGs, all the odd-order responses require time-reversal symmetry breaking while all the even-order effects require inversion symmetry breaking. The n -th order NLAH effect is contributed by the $(n-1)$ -th order moment of Berry curvature, which transforms as a rank- n pseudotensor. The details of the transformation properties of the Berry curvature multipoles can be found in the Supplemental Material [16], and the leading-order moments of the Berry curvature (therefore the leading-order intrinsic anomalous Hall responses) are obtained

accordingly [27], as listed in Table I. There are 32 MPGs (out of 122) which respect the combination of inversion and time-reversal symmetries \mathcal{IT} , forcing the Berry curvature to vanish in the entire Brillouin zone. Among the remaining 90 groups, 31 MPGs exhibit anomalous Hall effect, which can have nonzero spontaneous magnetization [26]. The 2nd-order NLAH effect is the leading-order Hall response in 39 MPGs and the 3rd-order NLAH effect is the leading response in 15 MPGs. There are 4 MPGs in which the hexapole is the leading-order moment, while in $m\bar{3}m$ MPG the octopole is the leading-order moment.

Similarly, we also study the leading-order response for the 31 MPGs in 2D space. The $(n+1)$ -th order NLAH effect is contributed by the n -th order moment of Berry curvature, which in 2D space has $n+1$ independent components: $\int_{\mathbf{k}} f_0 (\partial_x)^l (\partial_y)^{n-l} \Omega$, with $l = 0, 1, \dots, n$. By linear combination, they can be rearranged as $\int_{\mathbf{k}} f_0 \partial_+^{n-l} \partial_-^l \Omega$ with $\partial_{\pm} = \partial_x \pm i\partial_y$, which form the eigenvectors of the angular momentum operators, with quantum numbers $\pm n, \pm(n-2), \dots$. Apart from the zero angular momentum component, such as the monopole and the trace of quadrupole, all the other components are forced to vanish under a p -fold rotational symmetry with $p > n$. Therefore, if an additional time-reversal or mirror symmetry is present, which forces the zero angular momentum component to vanish, then the leading-order Berry curvature moment under a p -fold rotation has the order $n = p$, as shown in Table II. More detailed analysis can be found in the Supplemental Material [16], and the leading-order moments (therefore the leading-order intrinsic anomalous Hall responses) under all MPGs are listed in Table II. 10 MPGs (out of 31) respect the $C_2\mathcal{T}$ symmetry, which forces the Berry curvature to vanish in the entire Brillouin zone. Among the remaining 21 MPGs, 10 of them break both the time-reversal and mirror symmetry, therefore a non-vanishing monopole is allowed. The other 11 MPGs are also classified, according to their leading-order anomalous Hall responses.

Effective models.— In this section, we use an effective model to show explicitly how the quadrupole arises as the leading-order Berry curvature moment for materials with $4'mm'$ MPG in 2D space (as indicated by symmetry analysis in Table II). Importantly, $4'mm'$ is the symmetry for anti-ferromagnetic monolayer SrMnBi₂ which will be studied in detail in the next section. Furthermore, we show that the Berry curvature hexapole can be the leading-order moment for the surface states of topological insulators [28] with $3m1'$ (C_{3v}) MPG symmetry (see Table II).

The $4'mm'$ MPG contains two generators: $C_4\mathcal{T}$ and $M_x\mathcal{T}$, where C_4 is the four-fold rotation around the z axis and M_x is reflection: $x \rightarrow -x$. The $C_4\mathcal{T}$ requires the integration of Berry curvature to be zero, and $C_2 = (C_4\mathcal{T})^2$ also forces the dipole to vanish. In 2D space, since the Berry curvature is forced to align

TABLE II. Leading-order intrinsic anomalous Hall response in all the 31 2D magnetic point groups

leading-order response	magnetic point groups
No anomalous Hall response	$21', 2', 2mm1', 2'mm', 41', 4mm1', 61', 6', 6mm1', 6'm'm$
1st-order	$1, m', 2, 2m'm', 4, 4m'm', 3, 3m', 6, 6m'm'$
2nd-order	$11', m, m1'$
3rd-order	$2mm, 4', 4'mm'$
4th-order	$3m, 31', 3m1'$
5th-order	$4mm$
7th-order	$6mm$

along the z direction, the quadrupole can be denoted as $Q_{\alpha\beta} = \int_{\mathbf{k}} f_0 \partial_{\alpha} \partial_{\beta} \Omega_z$. There are three independent components of the quadrupole: Q_{xx}, Q_{yy}, Q_{xy} , and their physical meaning can be understood as follows. When an ac electric current is applied along the $x(y)$ direction, $Q_{xx}(Q_{yy})$ generates a third harmonic voltage in the $y(-x)$ direction. Furthermore, when the current is not applied along the two axes, Q_{xy} will have an additional contribution to the anomalous Hall voltage. The $C_4\mathcal{T}$ symmetry requires $Q_{xx} = -Q_{yy}$, and the $M_x\mathcal{T}$ symmetry further forces $Q_{xy} = 0$. Therefore, there is the only one independent non-vanishing component Q_{xx} in $4'mm'$ MPG.

Under $4'mm'$ MPG, we can write down an effective Hamiltonian up to the second-order in k near the Γ point:

$$\mathcal{H}(\mathbf{k}) = tk^2 + v(k_y\sigma_x - k_x\sigma_y) + m(k_x^2 - k_y^2)\sigma_z, \quad (14)$$

where σ denotes the Pauli matrices acting on the spin degrees of freedom, and $k = |\mathbf{k}|$. It is a Rashba-like Hamiltonian with a second-order warping term which breaks time-reversal symmetry. The $C_4\mathcal{T}$ symmetry forces the bands to be doubly degenerate at the Γ point. The energy spectra of the two bands are: $E_{\pm}(\mathbf{k}) = tk^2 \pm |\mathbf{d}(\mathbf{k})|$, as shown in Fig. 1(a). Here \pm denote the conduction and valence band respectively, and $\mathbf{d}(\mathbf{k}) = [vk_y, -vk_x, m(k_x^2 - k_y^2)]$.

The $C_4\mathcal{T}$ symmetry requires $\Omega_{\pm}(\hat{C}_4\hat{\mathcal{T}}\mathbf{k}) = -\Omega_{\pm}(\mathbf{k})$, leading to a clover-shape Berry curvature distribution as shown in Fig. 1(b), which is calculated as:

$$\Omega_{\pm}(\mathbf{k}) = \pm \frac{1}{2} \hat{\mathbf{d}} \cdot (\partial_x \hat{\mathbf{d}} \times \partial_y \hat{\mathbf{d}}) = \mp \frac{v^2 d_z(\mathbf{k})}{2|\mathbf{d}(\mathbf{k})|^3}. \quad (15)$$

Consider the situation when chemical potential μ is close to the band-crossing point: $|\mu| \ll \min\{\frac{v^2}{|t|}, \frac{v^2}{|m|}\}$,

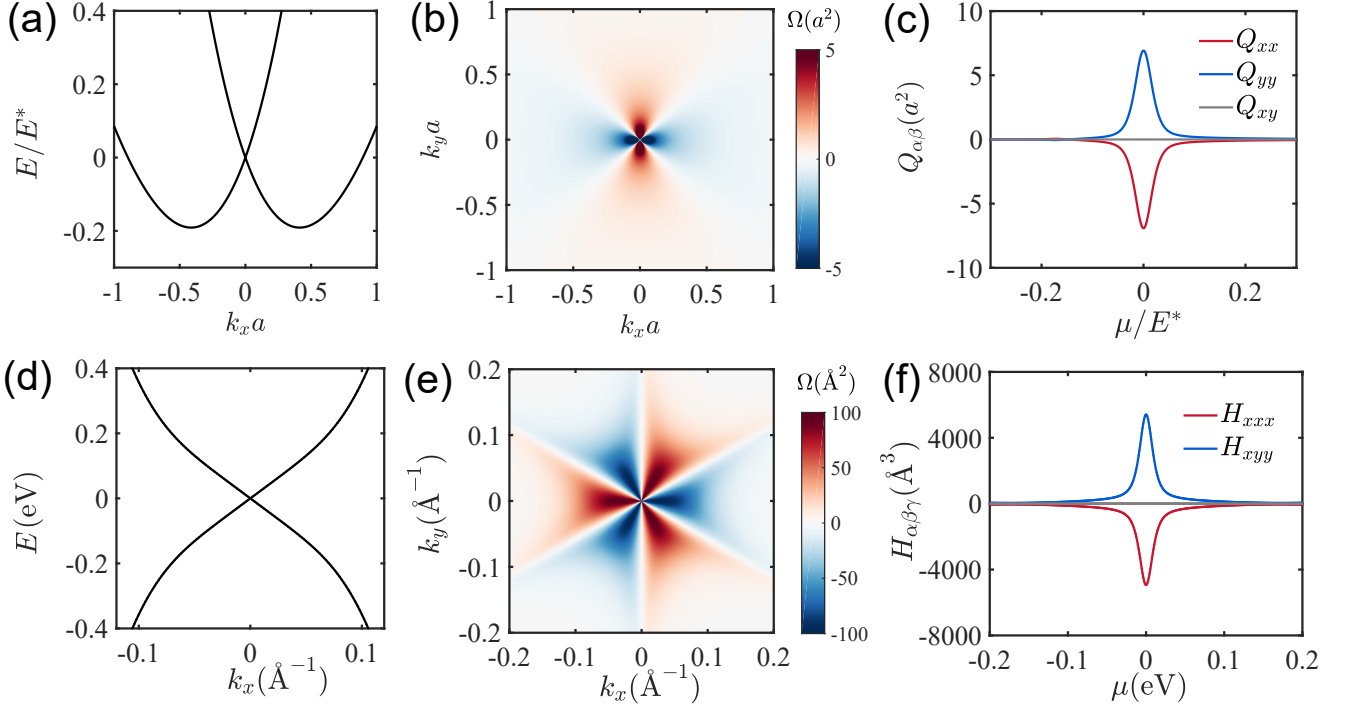


FIG. 1. (a)-(c) Band structures (a), Berry curvature of the conduction band (b) and gate dependence of the quadrupole (c) for the effective model in Eq. 14, with $t = 3$, $v = 1$, $m = 2$ and temperature $k_B T = 0.005$. The length scale $a = m/v$, and the energy scale $E^* = v^2/m$. (d)-(f) Band structures (d), Berry curvature of the conduction band (e) and gate dependence of the hexapole (f) for the surface states of topological insulators as described by Eq. 18. The parameters for Bi_2Te_3 are adopted from ref. [28], with $v = 2.55 \text{ eV} \cdot \text{\AA}$, $\lambda = 250 \text{ eV} \cdot \text{\AA}^3$, $E_0(k) = \alpha = 0$, and temperature $T = 50 \text{ K}$.

where the energy dispersion is approximately linear $E_{\pm}(\mathbf{k}) \approx \pm vk$, and the Berry curvature $\Omega_{\pm}(\mathbf{k}) \approx \mp \frac{d_z(\mathbf{k})}{2vk^3}$. The Berry curvature quadrupole at zero temperature can then be calculated with Eq. 11 as:

$$Q_{xx} = -Q_{yy} = -\frac{m}{16\pi|\mu|}, \quad (16)$$

$$Q_{xy} = 0. \quad (17)$$

The behaviour of the Berry curvature quadrupole is depicted in Fig. 1(c), which exhibits a peak near the band-crossing.

It is worth noting that the quadrupole is nearly the same for the conduction and valence band near the band-crossing at $\mu = 0$. Since near the band-crossing point where the kinetic term tk^2 can be neglected, the two bands have nearly opposite energy dispersions $E_+(\mathbf{k}) \approx -E_-(\mathbf{k})$, and opposite Berry curvatures $\Omega_+(\mathbf{k}) = -\Omega_-(\mathbf{k})$. According to Eq. 11, the quadrupole of the two bands are nearly the same around the band-crossing: $Q_{\alpha\beta}^+(\mu) \approx Q_{\alpha\beta}^-(-\mu)$.

Next, we study the Berry curvature hexapole for the surface states of topological insulators with $3m1'$ (C_{3v}) MPG. The time-reversal symmetry \mathcal{T} requires the monopole and quadrupole to be zero, and the C_3 symmetry also forces the dipole to vanish. In 2D space, the hexapole can be denoted as $H_{\alpha\beta\gamma} = \int_{\mathbf{k}} f_0 \partial_{\alpha} \partial_{\beta} \partial_{\gamma} \Omega_z$.

There are four independent components of the hexapole: H_{xxx} , H_{xxy} , H_{xyy} , H_{yyy} , and their physical meaning can be understood as follows. When an ac electric current is applied along the $x(y)$ direction, $H_{xxx}(H_{yyy})$ generates a fourth harmonic voltage in the $y(-x)$ direction. Furthermore, when the current is not applied along the two axes, H_{xxy} and H_{xyy} will have additional contributions to the anomalous Hall voltage. The C_3 symmetry requires $H_{xxx} = -H_{xyy}$, and the M_x symmetry further forces $H_{xxy} = H_{yyy} = 0$. Therefore, there is the only one independent non-vanishing component H_{xxx} in $3m1'$ (C_{3v}) MPG.

The effective Hamiltonian up to third-order of k which contains a hexagonal warping term is given by ref. [28]:

$$\mathcal{H}(\mathbf{k}) = E_0(k) + v_k(k_x \sigma_y - k_y \sigma_x) + \lambda k_x(k_x^2 - 3k_y^2) \sigma_z, \quad (18)$$

where $E_0(k) = \frac{k^2}{2m^*}$ is the kinetic energy. The velocity $v_k = v(1 + \alpha k^2)$ could have a second-order correction, which we will neglect near the Dirac point. The energy dispersion of the two bands are: $E_{\pm}(\mathbf{k}) = E_0(k) \pm |\mathbf{d}(\mathbf{k})|$, as shown in Fig. 1(d). Here $\mathbf{d}(\mathbf{k}) = [-vk_y, vk_x, \lambda k_x(k_x^2 - 3k_y^2)]$.

The Berry curvatures of the two bands can be calcu-

lated as:

$$\Omega_{\pm}(\mathbf{k}) = \pm \frac{1}{2} \hat{\mathbf{d}} \cdot (\partial_x \hat{\mathbf{d}} \times \partial_y \hat{\mathbf{d}}) = \mp \frac{v^2 d_z(\mathbf{k})}{|\mathbf{d}(\mathbf{k})|^3}, \quad (19)$$

and the Berry curvature of the conduction band is shown in Fig. 1(e).

When the chemical potential μ is close to the Dirac point: $|\mu| \ll \sqrt{\frac{v^3}{\lambda}}$, the energy dispersion is approximately linear $E_{\pm}(\mathbf{k}) \approx \pm vk$, and the Berry curvature $\Omega_{\pm}(\mathbf{k}) \approx \mp \frac{d_z(\mathbf{k})}{vk^3}$. The Berry curvature hexapole at zero temperature can then be calculated as:

$$H_{xxx} = -H_{xyy} = -\frac{3\lambda}{16\pi|\mu|}, \quad (20)$$

$$H_{xxy} = H_{yyx} = 0. \quad (21)$$

The behavior of the hexapole is depicted in Fig. 1(f), which has the same $|\mu|^{-1}$ dependence as the quadrupole in the antiferromagnetic model.

When a current is applied along the x direction which is perpendicular to the mirror plane, the hexapole will induce a NLAH voltage $V_y \propto H_{xxx} I_x^4$ along the y direction. As an estimation of the NLAH voltage for Bi_2Te_3 , we consider the situation when the Fermi energy is $\mu \approx 0.1$ eV away from the Dirac point of the surface state. Taking $\lambda = 250$ eV $\cdot \text{\AA}^3$ [28], we have hexapole $H_{xxx} = 150 \text{ \AA}^3$. Considering an applied electric current ~ 20 mA, with the conductance $\sim 2 \times 10^{-3} \Omega^{-1}$ for the surface states and the sample size ~ 1 mm [29], it corresponds to an electric field $E \sim 10$ mV/ μm . With the scattering time $\tau \sim 0.5$ ps [29], we obtain the NLAH current density $j^H(4\omega) \sim 20$ pA/mm, which corresponds to a Hall voltage ~ 10 nV.

Candidate materials.— In this section, we propose candidate materials to observe the third-order NLAH effect induced by Berry curvature quadrupole. Layered structure antiferromagnets AMnBi_2 ($A = \text{Sr, Ca, Ba, Eu}$) host anisotropic Dirac fermions near the Fermi surface [30–33]. Below the transition temperature, the MPG of bulk AMnBi_2 crystals is $4'/m'mm'$, which forces the bands to be doubly degenerate by the \mathcal{IT} symmetry. Single-domain thin-film SrMnBi_2 has been fabricated on $\text{LaAlO}_3(001)$ substrate [34], in which the \mathcal{IT} symmetry could be effectively broken by the substrate or vertical electrical gating, reducing the symmetry down to $4'mm'$ which supports nonzero quadrupole as its leading-order Berry curvature moment. To illustrate the symmetry breaking effect, here we study the Berry curvature quadrupole in monolayer (one sextuple layer) SrMnBi_2 with first-principles calculations.

The crystal structure of monolayer SrMnBi_2 is shown in Fig. 2(a). It contains a Mn layer which exhibits the antiferromagnetic order, and a conducting Bi layer which provides the Dirac fermions at the Fermi level [30]. The Dirac fermions are located along the $\Gamma - \text{M}$ lines, as indicated by the red dashed circle in Fig. 2(b). The \mathcal{IT}

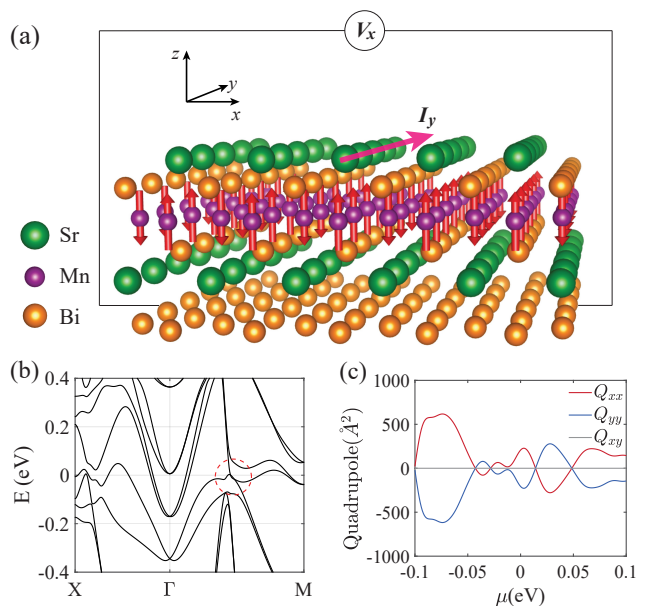


FIG. 2. (a) Crystal structure of monolayer (one sextuple layer) SrMnBi_2 , with the Mn atoms exhibit antiferromagnetic order as indicated by the red arrows. When a current is applied along the y direction, a NLAH voltage V_x will be induced by the Berry curvature quadrupole. (b) Band structures of monolayer SrMnBi_2 . Red dashed circle indicates the Dirac cone. (c) Berry curvature quadrupole of SrMnBi_2 near the Fermi level, with temperature $T = 100$ K.

symmetry coming from interlayer stacking in bulk crystals is absent in the monolayer, which lifts the two-fold degeneracy of the bands. Moreover, a small gap can be opened by the spin-orbit coupling [30], which generates Berry curvature near the band edges. When the chemical potential is near the Dirac point, sizable Berry curvature quadrupole $\sim 500 \text{ \AA}^2$ can be obtained, as shown in Fig. 2(c).

When an electric current is applied along the y direction, the quadrupole will induce a NLAH voltage $V_x \propto Q_{yy} I_y^3$ along the x direction, as shown in Fig. 2(a). As an estimation of the Hall voltage, we take an experimentally accessible current $\sim 100 \mu\text{A}$ [10, 11]. With the resistance ~ 1 k Ω [35], sample size $\sim 10 \mu\text{m}$, it corresponds to an applied electric field $E \sim 10$ mV/ μm . By taking the quadrupole $\sim 500 \text{ \AA}^2$ and the scattering time $\tau \sim 1$ ps, we obtain the NLAH current density $j^H(3\omega) \sim 1$ nA/ μm , corresponding to a Hall voltage $\sim 10 \mu\text{V}$, which is comparable with the nonlinear Hall voltage in WTe_2 [10, 11].

In ferromagnets, although the Berry curvature quadrupole is not the leading-order moment, it can still have contributions to the NLAH voltage. As the quadrupole contributes to the third harmonic generation, it could be distinguished from the anomalous Hall response with lock-in techniques. 2D magnets

MnBi₂Te₄ [36], Fe₃GeTe₂ [37], near 3/4-filling twisted bilayer graphene [38, 39] and 3D antiferromagnetic Weyl semimetals [40] Mn₃X (X = Ge, Sn, Ga, Ir, Rh, Pt) [3, 4, 6, 7, 41], GdPtBi [8] all have non-vanishing quadrupoles. Especially, MnBi₂Te₄ and twisted bilayer graphene exhibit quantum anomalous Hall effect [36, 38, 39, 42], which are therefore good platforms to study the Berry curvature effects. Sizable Berry curvature quadrupoles $\sim 4000 \text{ \AA}^2$ are found for twisted bilayer graphene near its ferromagnetic quantum anomalous Hall phase, as discussed in details in the Supplemental Material [16].

Discussions and conclusions.—In this work, we establish a general theory for the higher-order NLAH effects induced by Berry curvature multipoles. In particular, we point out that the third-order NLAH effect can be the leading-order Hall response in certain antiferromagnets, and the fourth-order NLAH can be the leading response in the surface states of topological insulators. We also propose candidate materials including 2D antiferromagnets and ferromagnets, Weyl semimetals and twisted bilayer graphene near the quantum anomalous Hall phase to observe the third-order NLAH effect.

Here, we further discuss several issues about the higher-order NLAH effects induced by Berry curvature multipoles. First of all, we discuss how to distinguish the NLAH responses related to the anti-symmetric part of the conductivity tensor from the Drude-like contributions which are related to the symmetric part of the conductivity tensor. For even-order responses, the Drude-like contribution is forbidden by the time-reversal symmetry, which is the case for the surface states of topological insulators. For odd-order responses, if a mirror symmetry M_x or $M_x\mathcal{T}$ is present, the Drude-like contribution vanishes in the transverse direction when the current is applied perpendicular to the mirror plane [14]. In monolayer SrMnBi₂ which belongs to $4'mm'$ MPG, the third-order Drude-like contribution vanishes when the current is applied along the x or y direction, as indicated in Fig. 2(a). In general cases, the NLAH responses can be distinguished from the Drude-like contributions as they have different angular dependences, and the details can be found in the Supplemental Material [16].

Second, we note that apart from the intrinsic contributions from Berry curvature, impurities can also give rise to the NLAH voltage through skew scattering and side jump [1, 18, 43]. Importantly, these contributions have the same symmetry properties [1, 18], thus will not affect the symmetry discussions in previous sections.

Third, besides the nonlinear Hall effect, it is shown that the Berry curvature dipole can induce other nonlinear effects such as the nonlinear Nernst [44, 45] and nonlinear thermal Hall effect [46]. Here, we believe that the Berry curvature multipole can also contribute to the corresponding higher-order nonlinear Nernst and nonlinear thermal Hall effects.

Acknowledgments.—The authors thank Benjamin T.

Zhou and Mengli Hu for valuable discussions. KTL acknowledges the support of the Croucher Foundation, the Dr. Tai-chin Lo Foundation and the HKRGC through grants C6025-19G, 16310219 and 16309718. HCP acknowledges support from a Pappalardo Fellowship at MIT.

* These authors contributed equally to this work

† phlaw@ust.hk

- [1] N. Nagaosa, J. Sinova, S. Onoda, A. H. MacDonald, and N. P. Ong, *Rev. Mod. Phys.* **82**, 1539 (2010).
- [2] D. Xiao, M.-C. Chang, and Q. Niu, *Rev. Mod. Phys.* **82**, 1959 (2010).
- [3] H. Chen, Q. Niu, and A. H. MacDonald, *Phys. Rev. Lett.* **112**, 017205 (2014).
- [4] J. Kübler and C. Felser, *Europhys. Lett.* **108**, 67001 (2014).
- [5] C. Stürgers, G. Fischer, P. Winkel, and H. v. Löhneysen, *Nat. Commun.* **5**, 3400 (2014).
- [6] S. Nakatsuji, N. Kiyohara, and T. Higo, *Nature (London)* **527**, 212 (2015).
- [7] A. K. Nayak, J. E. Fischer, Y. Sun, B. Yan, J. Karel, A. C. Komarek, C. Shekhar, N. Kumar, W. Schnelle, J. Kübler, C. Felser, and S. S. P. Parkin, *Sci. Adv.* **2**, e1501870 (2016).
- [8] T. Suzuki, R. Chisnell, A. Devarakonda, Y.-T. Liu, W. Feng, D. Xiao, J. W. Lynn, and J. G. Checkelsky, *Nat. Phys.* **12**, 1119 (2016).
- [9] I. Sodemann and L. Fu, *Phys. Rev. Lett.* **115**, 216806 (2015).
- [10] Q. Ma, S.-Y. Xu, H. Shen, D. MacNeill, V. Fatemi, T.-R. Chang, A. M. Mier Valdivia, S. Wu, Z. Du, C.-H. Hsu, S. Fang, Q. D. Gibson, K. Watanabe, T. Taniguchi, R. J. Cava, E. Kaxiras, H.-Z. Lu, H. Lin, L. Fu, N. Gedik, and P. Jarillo-Herrero, *Nature (London)* **565**, 337 (2019).
- [11] K. Kang, T. Li, E. Sohn, J. Shan, and K. F. Mak, *Nat. Mater.* **18**, 324 (2019).
- [12] M. Huang, Z. Wu, J. Hu, X. Cai, E. Li, L. An, X. Feng, Z. Ye, N. Lin, K. T. Law, and N. Wang, [arXiv:2006.05615](https://arxiv.org/abs/2006.05615).
- [13] J.-X. Hu, C.-P. Zhang, Y.-M. Xie, and K. T. Law, [arXiv:2004.14140](https://arxiv.org/abs/2004.14140).
- [14] D. E. Parker, T. Morimoto, J. Orenstein, and J. E. Moore, *Phys. Rev. B* **99**, 045121 (2019).
- [15] Furthermore, the prime symbol indicates that the spatial symmetries are combined with time-reversal operation.
- [16] See Supplemental Material for details of the DFT calculations, transport theory, symmetry analysis, Berry curvature quadrupole in quantum anomalous Hall materials, and angular dependences of NLAH effects and Drude-like contributions.
- [17] For example, $\tilde{\omega}$ represents $i\omega + \gamma$, $2\tilde{\omega}$ represents $2i\omega + \gamma$ and $-\tilde{\omega}$ represents $-i\omega + \gamma$. In the DC limit $\omega \ll \frac{1}{\tau}$, they can be simplified as $\tilde{\omega} \rightarrow \gamma = \tau^{-1}$.
- [18] S. Nandy and I. Sodemann, *Phys. Rev. B* **100**, 195117 (2019).
- [19] J.-S. You, S. Fang, S.-Y. Xu, E. Kaxiras, and T. Low, *Phys. Rev. B* **98**, 121109 (2018).
- [20] Y. Zhang, J. van den Brink, C. Felser, and B. Yan, 2D

- Mater.* **5**, 044001 (2018).
- [21] Y. Zhang, Y. Sun, and B. Yan, *Phys. Rev. B* **97**, 041101 (2018).
- [22] J. I. Facio, D. Efremov, K. Koepf, J.-S. You, I. Sodemann, and J. van den Brink, *Phys. Rev. Lett.* **121**, 246403 (2018).
- [23] Z. Z. Du, C. M. Wang, H.-Z. Lu, and X. C. Xie, *Phys. Rev. Lett.* **121**, 266601 (2018).
- [24] R. Battilomo, N. Scopigno, and C. Ortix, *Phys. Rev. Lett.* **123**, 196403 (2019).
- [25] B. T. Zhou, C.-P. Zhang, and K. Law, *Phys. Rev. Applied* **13**, 024053 (2020).
- [26] R. E. Newnham, *Properties of materials: anisotropy, symmetry, structure* (Oxford University Press, 2005).
- [27] S. V. Gallego, J. Etxebarria, L. Elcoro, E. S. Tasci, and J. M. Perez-Mato, *Acta Crystallogr. Sect. A* **75**, 438 (2019).
- [28] L. Fu, *Phys. Rev. Lett.* **103**, 266801 (2009).
- [29] D.-X. Qu, Y. S. Hor, J. Xiong, R. J. Cava, and N. P. Ong, *Science* **329**, 821 (2010).
- [30] J. Park, G. Lee, F. Wolff-Fabris, Y. Y. Koh, M. J. Eom, Y. K. Kim, M. A. Farhan, Y. J. Jo, C. Kim, J. H. Shim, and J. S. Kim, *Phys. Rev. Lett.* **107**, 126402 (2011).
- [31] K. Wang, D. Graf, L. Wang, H. Lei, S. W. Tozer, and C. Petrovic, *Phys. Rev. B* **85**, 041101 (2012).
- [32] L. Li, K. Wang, D. Graf, L. Wang, A. Wang, and C. Petrovic, *Phys. Rev. B* **93**, 115141 (2016).
- [33] H. Masuda, H. Sakai, M. Tokunaga, Y. Yamasaki, A. Miyake, J. Shiogai, S. Nakamura, S. Awaji, A. Tsukazaki, H. Nakao, Y. Murakami, T.-h. Arima, Y. Tokura, and S. Ishiwata, *Sci. Adv.* **2**, e1501117 (2016).
- [34] K. Takahashi, J. Shiogai, H. Inoue, S. Ito, S. Kimura, S. Awaji, and A. Tsukazaki, *AIP Adv.* **10**, 105216 (2020).
- [35] The resistivity of SrMnBi₂ is ~ 0.1 m Ω cm [30]. With a thickness of ~ 1 nm for monolayer, we estimate its resistance to be ~ 1 k Ω .
- [36] Y. Deng, Y. Yu, M. Z. Shi, Z. Guo, Z. Xu, J. Wang, X. H. Chen, and Y. Zhang, *Science* **367**, 895 (2020).
- [37] Y. Deng, Y. Yu, Y. Song, J. Zhang, N. Z. Wang, Z. Sun, Y. Yi, Y. Z. Wu, S. Wu, J. Zhu, J. Wang, X. H. Chen, and Y. Zhang, *Nature (London)* **563**, 94 (2018).
- [38] A. L. Sharpe, E. J. Fox, A. W. Barnard, J. Finney, K. Watanabe, T. Taniguchi, M. A. Kastner, and D. Goldhaber-Gordon, *Science* **365**, 605 (2019).
- [39] M. Serlin, C. L. Tschirhart, H. Polshyn, Y. Zhang, J. Zhu, K. Watanabe, T. Taniguchi, L. Balents, and A. F. Young, *Science* **367**, 900 (2020).
- [40] The Berry curvature quadrupole of Weyl semimetal Mn₃Sn is discussed in ref. [14].
- [41] Y. Zhang, Y. Sun, H. Yang, J. Železný, S. P. P. Parkin, C. Felser, and B. Yan, *Phys. Rev. B* **95**, 075128 (2017).
- [42] H. Fu, C.-X. Liu, and B. Yan, *Sci. Adv.* **6**, eaaz0948 (2020).
- [43] Z. Z. Du, C. M. Wang, S. Li, H.-Z. Lu, and X. C. Xie, *Nat. Commun.* **10**, 3047 (2019).
- [44] X.-Q. Yu, Z.-G. Zhu, J.-S. You, T. Low, and G. Su, *Phys. Rev. B* **99**, 201410 (2019).
- [45] C. Zeng, S. Nandy, A. Taraphder, and S. Tewari, *Phys. Rev. B* **100**, 245102 (2019).
- [46] C. Zeng, S. Nandy, and S. Tewari, *Phys. Rev. Research* **2**, 032066 (2020).